Effects of the Phoenix Lander descent thruster plume on the Martian surface

D. H. Plemmons,[1] M. Mehta,[2] B. C. Clark,[3] S. P. Kounaves,[4] L. L. Peach Jr.,[5] N. O. Renno,[2] L. Tamppari,[6] and S. M. M. Young[4]

Received 12 July 2007; accepted 6 May 2008; published 13 August 2008.

[1] The exhaust plume of Phoenix's hydrazine monopropellant pulsed descent thrusters will impact the surface of Mars during its descent and landing phase in the northern polar region. Experimental and computational studies have been performed to characterize the chemical compounds in the thruster exhausts. No undecomposed hydrazine is observed above the instrument detection limit of 0.2%. Forty-five percent ammonia is measured in the exhaust at steady state. Water vapor is observed at a level of 0.25%, consistent with fuel purity analysis results. Moreover, the dynamic interactions of the thruster plumes with the ground have been studied. Large pressure overshoots are produced at the ground during the ramp-up and ramp-down phases of the duty cycle of Phoenix's pulsed engines. These pressure overshoots are superimposed on the 10 Hz quasi-steady ground pressure perturbations with amplitude of about 5 kPa (at touchdown altitude) and have a maximum amplitude of about 20–40 kPa. A theoretical explanation for the physics that causes these pressure perturbations is briefly described in this article. The potential for soil erosion and uplifting at the landing site is also discussed. The objectives of the research described in this article are to provide empirical and theoretical data for the Phoenix Science Team to mitigate any potential problem. The data will also be used to ensure proper interpretation of the results from on-board scientific instrumentation when Martian soil samples are analyzed.

Citation: Plemmons, D. H., M. Mehta, B. C. Clark, S. P. Kounaves, L. L. Peach Jr., N. O. Renno, L. Tamppari, and S. M. M. Young (2008), Effects of the Phoenix Lander descent thruster plume on the Martian surface, *J. Geophys. Res.*, *113*, E00A11, doi:10.1029/2007JE003059.

1. Introduction

[2] The final descent and touchdown phase of the Phoenix Lander is controlled by twelve hydrazine (N_2H_4) monopropellant retro-rocket engines in pulsed mode, which could result in the impingement of some of the exhaust products onto the Martian regolith at the landing site during the landing phase. The Phoenix engines use pulse frequency and duty cycle control to dynamically throttle power during descent [*Wong and Masciarelli*, 2002].

[3] There is concern among the Phoenix Science Team that the exhaust products could interact with and alter the natural compounds in the Martian soil. There is also concern that the undecomposed hydrazine and potential impurities in the fuel could contaminate the landing site. Finally, site alteration and dust lifting by the interaction of the pulsed jet with the Martian regolith is also a potential concern.

[4] To address these issues, the Phoenix Science Team has performed extensive analysis of the hydrazine fuel, the thruster exhaust products, and the dynamical interaction of the exhaust plume with the ground surface. These efforts included (1) selecting the cleanest, driest propellant available for the mission; (2) assaying and documentation of the mission propellant; (3) conducting experimental plume signature identification during the hot fire engine qualification testing of the flight motors using a batch of the mission propellant; (4) capturing sample exhaust gases from these tests for use in future laboratory analysis; (5) extensive laboratory testing, computational modeling and analysis; and (6) preserving a batch of the mission propellant and a back-up rocket motor for potential future testing, should this be warranted. Computational and experimental studies have been performed on the products of the catalytic hydrazine decomposition in order to understand the potential physical interactions of the rocket plume with the Martian surface.

[5] A very brief discussion of two of the Phoenix Lander primary scientific instruments that will benefit from the plume diagnostics data and analysis efforts is included in this section to provide some context for this investigation. A

[1] Aerospace Testing Alliance, Arnold Air Force Base, Tennessee, USA.
[2] Department of Atmospheric, Oceanic and Space Sciences, University of Michigan, Ann Arbor, Michigan, USA.
[3] Lockheed Martin Corporation, Littleton, Colorado, USA.
[4] Department of Chemistry, Tufts University, Medford, Massachusetts, USA.
[5] Universities Space Research Association, Columbia, Maryland, USA.
[6] Jet Propulsion Laboratory, California Institute of Technology, Pasadena, California, USA.

0148-0227/08/2007JE003059

more detailed description of these instruments is included in other manuscripts in this special issue [*Kounaves et al.*, 2008; W. V. Boynton et al., The Thermal and Evolved-Gas Analyzer on the Phoenix Mars lander, manuscript in preparation, 2008].

[6] The Microscopy, Electrochemistry and Conductivity Analyzer (MECA) is a combination of scientific instruments including a wet chemistry laboratory (WCL), optical and atomic force microscopes, and a thermal and electrical conductivity probe. MECA will determine acidity, saltiness, and composition by mixing soil samples with small amounts of water. MECA will also examine the soil grains to provide information on mineralogy and origin.

[7] The Thermal and Evolved Gas Analyzer (TEGA) is a combination of high-temperature ovens and a mass spectrometer that will be used to perform chemical analysis of Martian soil and ice samples. TEGA will be used to detect volatiles, soil mineralogy, and potential organics that may be resident on the Martian surface.

[8] Understanding the physics of rocket plume impingement on planetary surfaces is important for the survivability of the spacecraft during terminal descent and touchdown phases of Entry, Descent and Landing (EDL) [*Albee et al.*, 2000].

[9] Limited investigations of steady state rocket plume interactions with the Martian soil surface were conducted for the Viking mission by NASA researchers in the 1970s [*Grover et al.*, 2005]. The dynamics of the interaction of an underexpanded jet plume flow field, where the nozzle exit pressure is greater than the ambient (back) pressure, with the surface is quite complex. Indeed, instabilities in the flow occur because of the coexistence of subsonic, transonic, and supersonic regions within the flow [*Krothapalli et al.*, 1999]. For this reason, computational simulations must be tested with data from experiments [*Janos and Hoffman*, 1968].

[10] This paper discusses the objectives of plume diagnostics research efforts and explains why they are important to the Phoenix science mission. We present the methodology and results from three research efforts: (1) spectral diagnostics of the rocket engine exhaust gases, (2) analysis of plume gases using gas chromatography and mass spectrometry, and (3) physical interactions of the rocket plume with the regolith. We conclude with a brief discussion on planned future work and how these data will help with the scientific measurements on Mars.

2. Objectives

[11] The understanding of the physical interaction of thruster plumes with the Martian surface is also crucial for assessments of dust lifting and spacecraft contamination. However, detailed experimental investigations of pulsed rocket plume interaction with the ground and the Martian regolith are currently not available [*Mehta et al.*, 2007]. We conducted computational simulations and laboratory experiments to study these interactions and assess their effects on dust lifting. We report such measurements here and show that they are consistent with numerical simulations. The hydrazine fuel used in the Phoenix Lander is high purity grade (99% by weight) but still contains impurities such as water (<1%), ammonia (<0.3%), aniline (<0.003%), and trace organics (<0.005%). There was a significant level of uncertainty among the science team as to the exact composition of the exhaust products and it was decided to perform additional experimental and numerical studies on the Phoenix landing system rocket engines.

[12] The objectives of this research are to determine the chemical compounds present in the rocket engine exhaust and to characterize the physical interaction of the thrusters exhaust plumes with the Martian surface. The affects of the exhaust products on the inorganic chemical analysis will be addressed in a separate paper.

3. Plume Gas Sampling and Analysis Using Fourier Transform Infrared Diagnostics

3.1. Chemical Reaction Modeling

[13] The primary product of hydrazine decomposition is ammonia

$$3N_2H_4 \rightarrow 4NH_3 + N_2. \quad (1)$$

In the presence of sufficient heat, the ammonia will further decompose into N_2 and H_2

$$2NH_3 \rightarrow N_2 + 3H_2. \quad (2)$$

The catalyst beds in the Phoenix landing system engines are made of iridium and rhodium metals affixed to a porous ceramic alumina. The decomposition of N_2H_4 with an iridium catalyst can be expressed by [*Lyon*, 1971]

$$N_2H_4 \rightarrow 4/3(1-x)NH_3 + 1/3(1+2x)N_2 + 2xH_2, \quad (3)$$

where x is the fraction of originally formed ammonia that has dissociated into N_2 and H_2. A rhodium catalyst produces nitrogen and hydrogen in equal quantities [*Sayer*, 1970]

$$2N_2H_4 \rightarrow 2NH_3 + N_2 + H_2. \quad (4)$$

[14] Chemical equilibrium modeling was performed to provide some insight on interpretation of equations (1)–(4). The predicted plume properties are shown in Table 1. The equilibrium model column in Table 1 is the output from the NASA Gordon-McBride [*McBride and Gordon*, 1996] chemical equilibrium code. The quenched model column in Table 1 is the results from similar calculation performed by the engine manufacturer. The manufacturer's code is a modified version of the Gordon-McBride code that allows for quenching the NH_3 decomposition inside the combustor. Equations (1)–(4) show that the products in hydrazine monopropellant rocket exhaust plume can significantly vary, with possible major species mole fractions of NH_3 10%–80%, H_2 0%–67%, N_2 20%–33%, and N_2H_4 unknown.

[15] As mentioned in the section 2, the hydrazine fuel used in the Phoenix Lander is high purity grade. A purity analysis was performed by the engine manufacturer to ensure that the fuel was in compliance with military specification MIL-P-26536. The results from the purity analysis are shown in Table 2.

Table 1. Chemical Equilibrium Calculated Mole Percent at the Rocket Engine Nozzle Exit

Species	Equilibrium Model	Quenched Model
NH_3	9.1%	36%
N_2	32%	27%
H_2	59%	36%

3.2. Test Procedure

[16] The thrusters exhaust products were characterized during the operational test phase of the engine manufacturing process. Three plume analysis systems were used (in addition to modeling and simulation) to ensure thorough characterization of the exhaust products. Exhaust gas samples were extracted through a heated sample line and analyzed using a Fourier transform infrared (FTIR) multigas analyzer (MGA) [*Markham et al.*, 2004]. A separate plume sample was extracted through the heated sample lines and stored in a passivated sample canister for off-site analysis using gas chromatography/mass spectrometry (GC/MS) methods. An additional gas sample was collected and stored for future analysis, if required. An instrumentation schematic is shown in Figure 1.

[17] As mentioned in the Introduction, the same fuel lot as used on board the Phoenix Lander was used during the engine test firings. The results from the MGA analysis were previously reported by *Plemmons et al.* [2007] and are summarized below.

3.3. Plume Analysis Results

[18] On the basis of the hydrazine decomposition analysis, the concern over unreacted hydrazine, and the results from the fuel purity analysis, the FTIR MGA was calibrated to measure high levels of NH_3, and low levels N_2H_4, and water vapor. Exhaust gas samples were acquired and analyzed for two separate engine firings. The MGA measured NH_3 concentrations in excess of 50% during engine start and settled to 45% after the engine reached operating temperature, which is 19% higher than the engine manufacturer's performance model and 5 times larger than the equilibrium model prediction. The measured water vapor levels are just under 0.25%, which is in agreement with the pretest fuel purity analysis shown in Table 2 and indicates that water does not participate significantly in the reaction.

[19] No hydrazine was observed in the thruster exhaust plume. However, the hydrazine FTIR absorption features on this instrument are coincident with the ammonia absorption spectra. Hence, the high ammonia concentration will mask low concentration hydrazine. On the basis of posttest analysis of the FTIR spectra where the spectra were manually searched for hydrazine absorption features, it is estimated that the unreacted hydrazine levels in the thruster plume is less than 0.2%.

[20] The ammonia and water vapor concentration measured for one of the engine firings is shown in Figure 2. The engine was fired for approximately 40 s. At the end of the firing, the FTIR absorption cell was isolated and the MGA continued to analyze the final sample to obtain a baseline estimate on the instrument precision under test conditions. After approximately 2 min 40 s, the absorption cell was purged with high-purity nitrogen and the ammonia and water vapor concentration readings returned to zero.

[21] Gas samples were extracted from the exhaust plume of two Phoenix retrorocket thrusters during hot fire acceptance testing. Recirculation gas samples were taken from inside the test cell for two additional engine firings. The samples were analyzed for ammonia, water vapor, and hydrazine concentrations using a FTIR absorption spectrometer. The measured ammonia and water vapor were in reasonable agreement with expected values. Using a value of $x = 0.3$ in equation (3), yields 45% NH_3, 26% N_2, and 29% H_2, on a molar basis.

4. Analysis of the Plume Gases Using Gas Chromatography–Mass Spectrometer

[22] The purpose of this analysis was to corroborate the spectroscopic infrared gas analysis via the gas sample probe that was performed during the test firings. The samples were obtained during the test firings by diverting the plume gases into two passivated gas sample canisters. One was charged with the plume gases at 300 torr and the other at 1,277 torr, respectively. The analysis reported here was performed using the 1,277 torr sample. The analytical procedures for the instrumental analysis were developed for simple sample extraction, and used standard methods on a standard configuration GC-MS. The 300 torr sample and the remaining 1,170 torr sample have been stored for future testing should specific questions arise during surface measurements on Mars or should they arise regarding interpretation of the chemistry results.

4.1. Analytical Methodology

[23] During two of the test firings, the stainless steel heated sample lines carrying hot rocket exhausted gases outside the test chamber, through a heated boost pump, delivered the gases to a sample canister rather than to the FTIR-MGA instrument. One of those sample containers collected only 300 torr of exhaust gases. Since this is below atmospheric pressure, the sample can only be accessed through complicated line work and was thus not analyzed in these tests. The other sample canister collected at a pressure of 1,277 torr, well above 760 torr (1 atm) was easily extracted and required no complicated processing.

[24] A septum was attached to the canister outlet. The attachment included a rubber stopper plate through which a syringe could be inserted to extract samples. A small space of less than 0.25 mL volume was formed between the stopper and the closed valve of the canister. The canister

Table 2. Hydrazine Purity Analysis Results

Compound	Acceptable Values for High Purity Grade (by Weight)	Measured Values
N_2H_4	99.00% min	99.69%
H_2O	1.00% max	0.25%
NH_3	0.30% max	0.06%
Trace Organics (Excluding Aniline)	0.005% max	0.001%
Aniline	0.003% max	<0.0006%
Total Nonvolatiles	0.0010% max	0.0004%
Particulates	1 mg L^{-1} max	0.8 mg L^{-1}
Corrosivity	0.00125% Fe max	0.00025%
Chlorine	0.0005% max	0.00017%
CO_2	0.0030% max	0.0003%

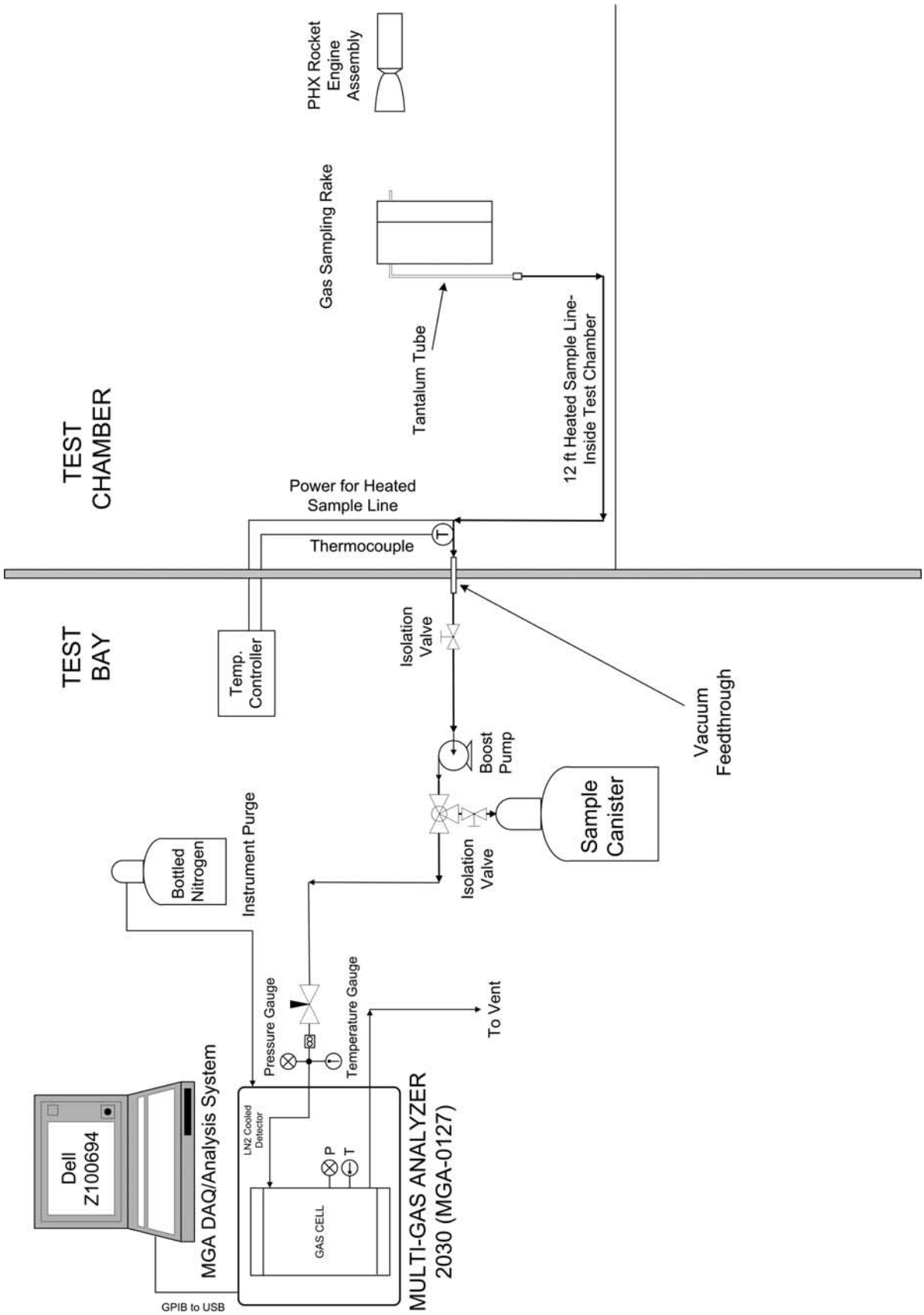

Figure 1. Schematic of the FTIR instrumentation installed on the rocket engine test cell.

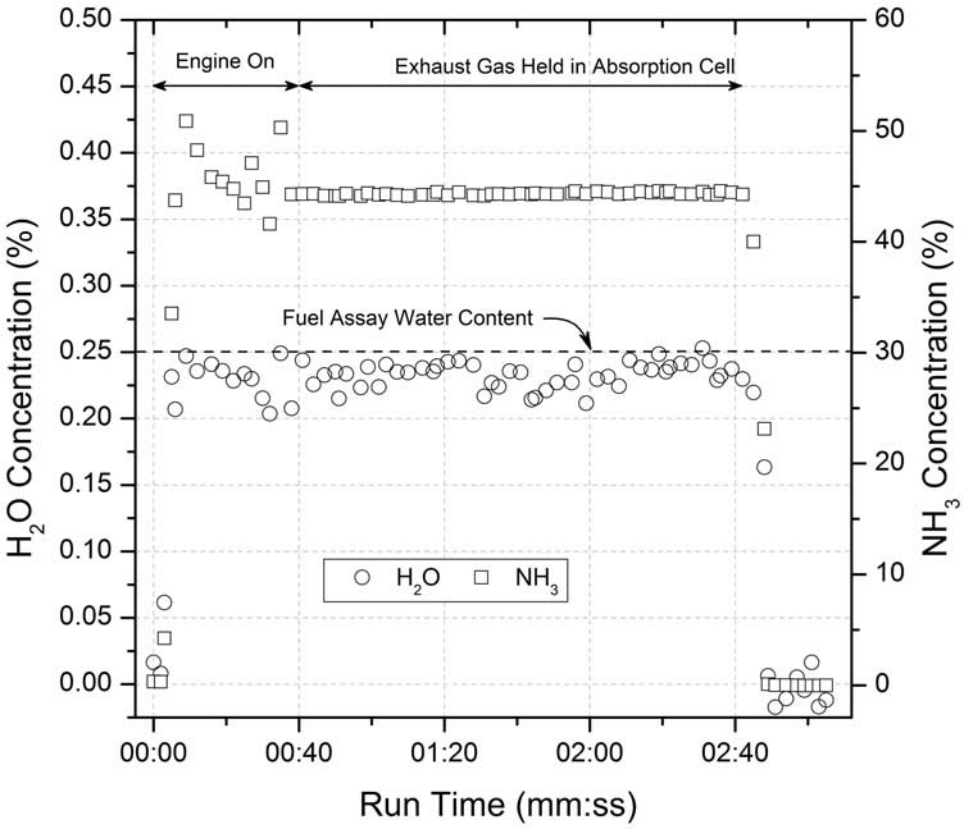

Figure 2. Multigas analyzer results for ammonia and water vapor.

had to be opened and bled significantly (3 or 4 times for several seconds) to flush air out of the chamber. Samples were tested each time. The oxygen peak reduced significantly with each flush. When the oxygen peak disappeared, it was assumed the chamber was emptied of air.

[25] With the septum closed tight and the canister fully open, the small chamber was allowed to come to equilibrium with the gases in the canister. The canister was then fully closed off from the chamber. A 100 μL sample was extracted from the chamber, through the septum, with a 500 μL (Superco SGE) gas tight syringe. The sample was carried 15 feet and manually injected into the GC-MS (Shimaduz QP-5050A).

[26] The injection temperature was 200°C and interface temperature 280°C. The instrument control mode was split because the samples were large and plentiful. The total flow rate was 21.7 mL min^{-1} under an inlet pressure of 100 kPa. The final reported analyses were run for 5 min at a steady oven temperature of 50°C. Higher temperatures and ramped temperatures were unnecessary since the entire sample was gaseous and did not need to be volatilized. With significantly longer runs (>1 h) only the peak at 1.25 min was observed in the gas chromatogram and thus a 5 min run was more than sufficient.

[27] Prior to the sample analysis, air was run by identical sample delivery and GC-MS method. The GC-MS method was also run without injection of any sample, and provided a true blank. After all plume analyses were complete, the GC-MS was baked out using a very slow temperature ramp of 50°C to 470°C. There were no indications of any less volatile substances remaining on the column.

4.2. GC-MS Results

[28] Table 3 shows the results for the mass spectrum of the air blank and plume sample. The blank, containing approximately 77% N_2 and 21% O_2, displays a mass peaks at 28 m/z (14 + 14 atomic mass units (amu)) with a relative intensity (I_{rel}) of 100 and at 32 m/z (16 + 16 amu) with an I_{rel} = 40.4.

[29] The chromatogram for the 100 μL plume sample shows a single sharp peak with a retention time of 1.2 min. This peak in turn resulted in a mass spectrum with three major peaks at 16m/z (I_{rel} = 88.8), 17m/z (I_{rel} = 100), and 28 m/z (I_{rel} = 75.6). These peaks can be assigned to NH_2 (16 amu), NH_3 (17 amu), and N_2 (28 m/z), respectively. Other very minor ammonia-related and water peaks are also present, probably for NH (15 amu) and H_2O (18 amu). It should be noted that detection and analysis of H_2 is extremely complex and requires special containers, handling, and procedures; thus no attempt was made to measure the H_2 content of the plume gases. It is also important to note that no standards were used to construct calibration

Table 3. Results of GC-MS Analysis

m/z	Air, I_{rel}	Sample, I_{rel}	Fragment
15	0.0	5.2	NH
16	3.1	88.8	NH_2
17	0.4	100.0	NH_3
18	0.8	3.8	? H_2O, NH_4
28	100.0	75.6	N_2
31	0.0	0.0	
32	40.4	1.2	O_2

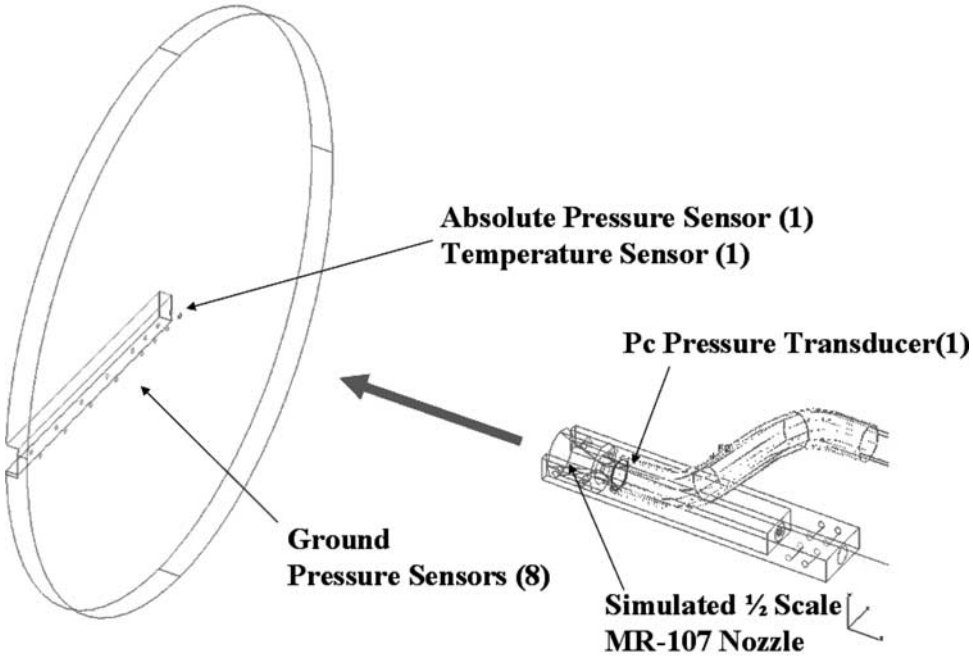

Figure 3. Schematic of the CFTB experimental setup [*Mehta et al.*, 2007].

curves and thus no quantitative results are provided for any of the other constituents.

4.3. Interpretation of GC-MS Results

[30] The most significant results of the GC-MS analysis are (1) that a major fraction of the thruster plume is composed of NH_3 and (2) that no hydrazine is present. As discussed above, the quenched equilibrium code for the Phoenix hydrazine thrusters predicts 36% NH_3, 36% H_2, and 27% N_2. The in situ plume gas analysis yielded 45% NH_3 and 0.23% H_2O. Using absolute intensities and setting the level of NH_3 + NH_2 + NH at 45%, we can calculate the levels of N_2 and H_2O, as 18% and 0.8%, respectively. Even though our results are not rigorously quantitative, these levels are reasonably close to those predicted by the model and performance criteria. Taking into account all these results, it is reasonable to estimate that the plume contains about 45% (±5%) NH_3.

[31] The more significant result is that we found no indication in the mass spectrum, within our detection limits, of N_2H_4 (32 amu). If any is present it is <1%, however, given that there is no confirmation peak at 31amu for N_2H_3, the peak at 32 amu is most likely due to O_2 contamination from air not fully evacuated from the container.

[32] The other major reaction product found in the plume sample is N_2. This can typically range from 20% to 35% and the model predicts 27%. Our estimated result of 18% is low, but can be accounted for by the errors introduced if we allow for some recombination of N_2 and H_2 fragments to give NH.

5. Flow Physics of Pulsed Rocket Plume Impingement at Mars Pressure

[33] We developed and tested an experimental facility to simulate the flow physics of the Phoenix pulsed rocket engine and its interaction with the Martian surface. Indeed, all requirements for simulating the physical interaction of the rocket plume with the hard ground were determined using nondimensional scaling parameters. Numerical simulations were used to help the physical interpretation of the experimental results.

5.1. Experimental and Computational Methodologies

5.1.1. Experimental Methodology

[34] The University of Michigan developed a cold flow (nonheated jet) test bed (CFTB) to study the impingement of supersonic pulsed jets on a flat surface at Mars ambient pressure (Figure 3). The thruster firing frequency, the duration of the pressure pulse, and the chamber pressure (P_C) were adjustable. Dry compressed nitrogen gas at room temperature was used to simulate hydrazine decomposition products because it has a similar specific heat capacity ratio. Fast response microelectromechanical system (MEMS) pressure sensors were placed radially across the impingement plate at a spacing distance of 27.5 mm between sensors. One thermocouple was also placed at the plate's centerline. One 1/2 scale thruster with a similar nozzle contour profile as the Phoenix MR-107 descent engine nozzle was mounted inside a thermal vacuum chamber, which was set to an ambient pressure of 690 Pa and ambient temperature of 290 K. During the constant velocity descent phase of the Phoenix spacecraft, the rocket plumes are pulsed at a 10 Hz frequency, with a 45 ms pulse width, a maximum chamber pressure ($P_{C\text{-}max}$) of 1.24 MPa, and a chamber pressure (P_C) rate of change during engine startup/shutdown cycles of approximately 152 MPa s^{-1}. Our CFTB system met all these requirements. The thruster chamber pressure and the ground impingement pressures (P_s) were measured at a sampling rate of 48 kHz. The thruster altitude (i.e., the distance of the thrusters from the impingement plate) can be adjusted from 0.25 m (touchdown altitude) to 2 m above the simulated surface.

5.1.2. Scaling Laws for Rocket Plume Flow Physics

[35] We used scaling laws to match the physics of our CFTB to that of the actual thruster exhaust plume. The three scaling parameters that we used are the Mach similarity parameter (k), the expansion ratio (e), and the exit total pressure ratio (α). The Mach similarity parameter is defined as the ratio of the kinetic energy of the plume to the internal energy of the plume at the nozzle exit [*Land and Scholl*, 1966],

$$k = \gamma(\gamma - 1)M^2 \tag{5}$$

where γ is the specific heat ratio and M is the exit Mach number. Matching the Mach similarity parameter of our CFTB to that of the rocket exhaust plume ensures that the flow physics associated with the two jets are similar.

[36] The other parameter that we used to scale our CFTB is the expansion ratio of the exhaust plume at the nozzle exit. This parameter is empirically related to the expansion angle of the plume with respect to the centerline. This in turn is determined by the ratio of nozzle exit pressure (P_e) to ambient pressure (P_∞) [*Clark and Conner*, 1969],

$$e = \frac{P_e}{P_\infty}. \tag{6}$$

The final scaling parameter that we used is the total pressure ratio at the nozzle (α). This parameter is obtained by nondimensionalizing the total pressure of the exhaust plume at the nozzle exit (P_{oe}) with respect to the maximum thruster chamber pressure ($P_{C\text{-}max}$). That is (M. Mehta and N. O. Renno, Ground interaction dynamics of pulsed supersonic underexpanded jets at low ambient pressure, manuscript in preparation, 2008),

$$\alpha = \frac{P_{oe}}{P_{C-\max}}. \tag{7}$$

The total pressure ratio derived from one-dimensional isentropic flow equations at the nozzle exit is an important parameter in ensuring that the CFTB has ground pressure profiles similar to the full-scale case of the real size and performance of the rocket motor. The thruster plume temperature is not critical in understanding the force loads on the surface [*Roberts et al.*, 1982], provided the appropriate test gas is used (M. Mehta and N. O. Renno, manuscript in preparation, 2008).

[37] By matching the scaling parameters k, e, and α, and the geometric length scaling with respect to the nozzle diameter, the shock and impingement flow structures produced by our CFTB accurately simulate those produced by the rocket exhaust (M. Mehta and N. O. Renno, manuscript in preparation, 2008). Table 4 quantitatively compares nondimensional plume parameters between the experimental setup and the full scale. The rocket exhaust parameters vary depending on the extent of ammonia disassociation during the hydrazine decomposition reaction described in section 3.3 [*Plemmons et al.*, 2007].

5.1.3. Computational Methodology

[38] In addition to the experimental study, we also used axisymmetric computational fluid dynamics (CFD) models to study the transient impingement of the Phoenix thruster plume on the surface. Unsteady, compressible inviscid and turbulent numerical solvers of the finite volume based ANSYS Inc. FLUENT code were used. Structured mesh generation was developed for the flow domain using ANSYS Gambit. Grid adaptation and an iterative time stepping size of 1 μs were applied to the computational models to resolve shocks and capture small transient events. This CFD study was done in collaboration with Lockheed Martin's Aerophysics Department. Time series of thruster chamber pressure measured during hot fire (rocket engine testing) and cold flow tests were used to force the CFD models [*Huseman and Bomba*, 2000].

Table 4. Exhaust Plume Nondimensional Scaling Parameters

Parameters	Full Scale	Experiment
k	7.5–12.7	12.7
e	4–7	4.4
α	0.51–0.45	0.59

5.2. Experimental Results

[39] The main data obtained from our experiments were the P_C and ground pressure time series and spatial ground pressure profiles. From temporal ground pressure profiles at touchdown altitude (Figure 4), the centerline peak pressures at the ground vary between 35 and 20 kPa (nondimensional ground pressure values of 0.028 and 0.014, respectively). These surface pressure overshoots last between 10 and 18 ms (Figure 4), which is repeatable for the two 100 ms pulse firing sequences. The P_C pulse firing sequence comprises of: 10–12 ms P_C ramp up; 40–50 ms of relatively constant maximum P_C value known as the quasi-steady state regime; and 30 ms P_C ramp down (Figure 4). The pressure amplitude is largest at the centerline (Figure 4) and it decreases nonlinearly with distance of the thruster from the surface (not shown) (M. Mehta and N. O. Renno, manuscript in preparation, 2008). During the quasi-steady state regime, at nondimensional altitude of $h/D_e = 8.4$, the pressure amplitude is about 5 kPa ($P_s/P_{C\text{-}max} = 0.005$) for about 40 to 50 ms into each power cycle. As can be seen from the back pressure profiles, we are only able to capture two thruster firing cycles due to a significant increase in the vacuum chamber ambient pressure which alters the ground pressure and jet shock structure (M. Mehta and N. O. Renno, manuscript in preparation, 2008). The large transient ground overpressures illustrated in Figure 4 do not occur in experiments with steady state (nonpulsating) thruster plumes (not shown) (M. Mehta and N. O. Renno, manuscript in preparation, 2008). The physical reason for this difference is explained in more detail below, because these ground pressure overshoots play an important role in soil erosion.

[40] Further evidence of ground pressure overshoots are seen in the spatial ground pressure profiles presented in Figure 5. It shows that at t = 112 ms, around the time of the first pressure overshoot during the second firing cycle, the centerline pressure amplitude is 16 kPa ($P_s/P_{C\text{-}max} = 0.013$) and that during the quasi-steady state phase at t = 136 ms the pressure amplitude decreases to 5 kPa ($P_s/P_{C\text{-}max} = 0.0042$). It can be seen that during the quasi-steady state regime, the ground pressure is relatively constant up to approximately r/D_e of 0.9 and then it decreases monotonically.

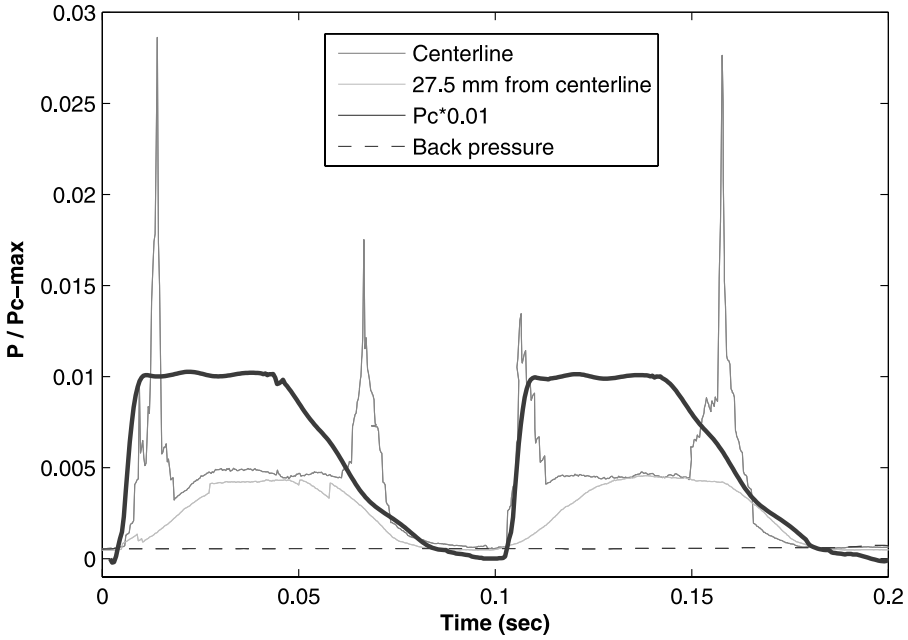

Figure 4. Nondimensional thruster chamber pressure (P_C) and ground pressure (P_s) time series during two complete 45 ms pulse width thruster firing cycles at the Phoenix touchdown altitude (h/D_e = 8.4). The plot shows the ground pressure profiles at the thruster centerline and at a radial distance 27.5 mm from the centerline, the ambient (back) pressure, and the P_C time series. The quasi-steady state regime occurs between 20 and 60 ms for the first firing cycle and between 115 and 150 ms for the second firing cycle. For the first engine cycle, plate shock formation occurs between 10 and 25 ms and approximately between 70 and 85 ms during plate shock collapse.

5.3. Numerical Results

[41] Figure 6a shows the Mach contour-time sequence profiles of a pulsed supersonic jet impinging on a flat surface at an altitude of h/D_e = 25. These calculations were done at Mars ambient pressure conditions and ambient temperature of 298 K. The plume properties were those of dry nitrogen at temperature of approximately 300 K, similar to the experimental conditions. Similar characteristic tran-

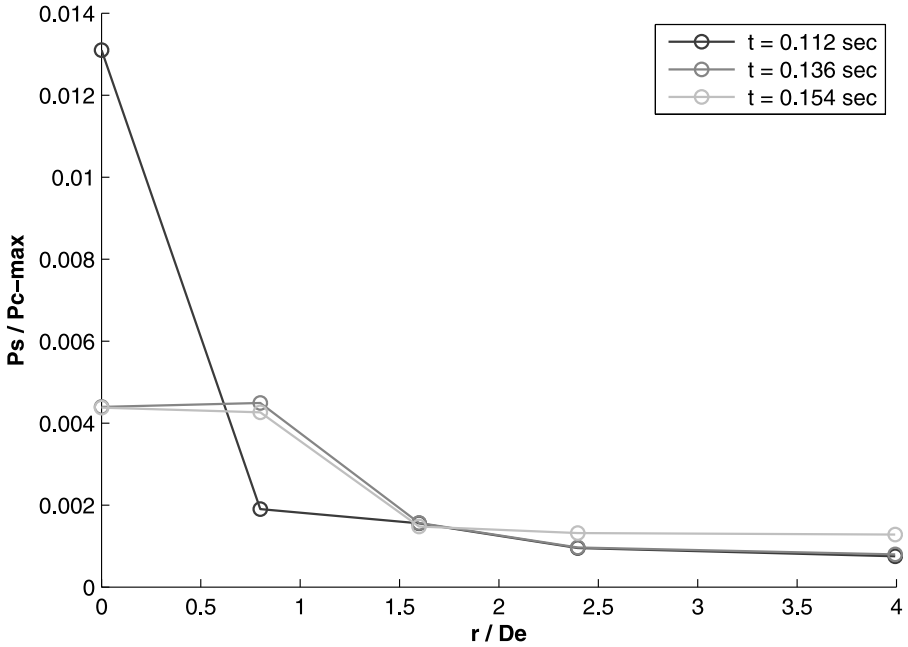

Figure 5. Ground pressure profile (P_s) nondimensionalized with the maximum chamber pressure ($P_{c\text{-}max}$), as a function of nondimensional distance from the centerline at the ground in two phases of the thruster firing cycle at an altitude of h/D_e = 8.4: before (112 ms) and during (136 ms; 154 ms) fully developed plate shock formation.

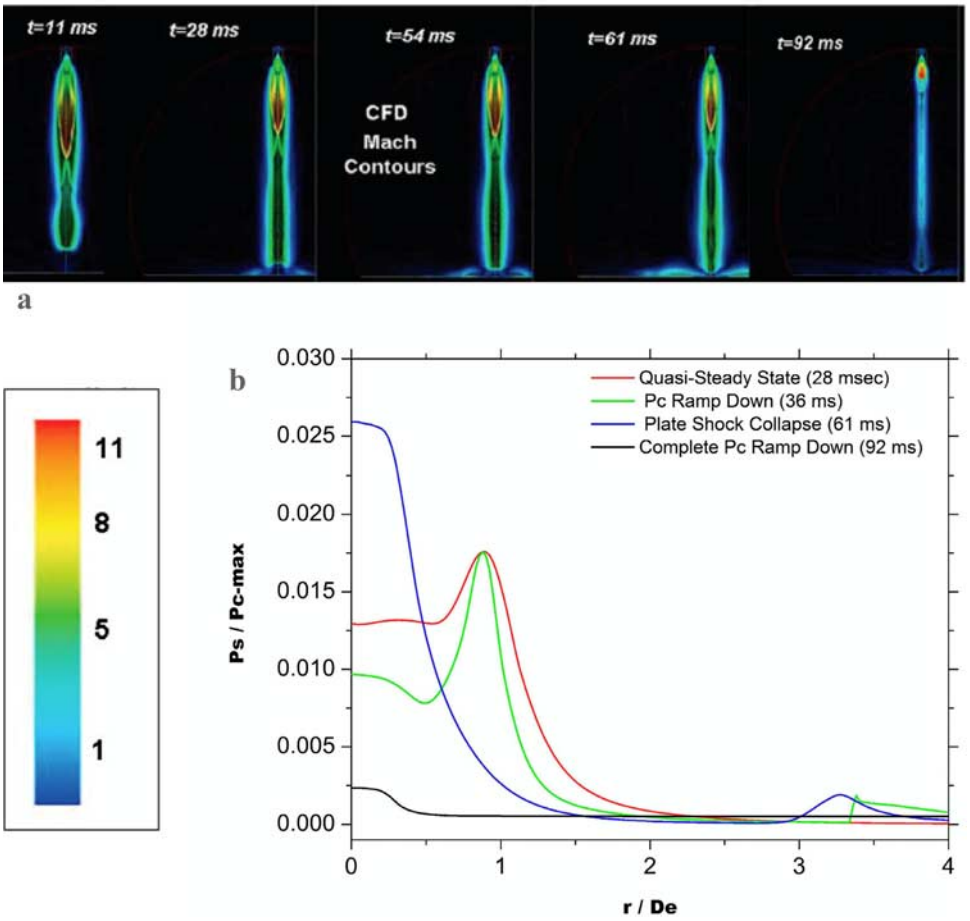

Figure 6. Plate shock formation and collapse process at h/D_e = 25 from axisymmetric, inviscid, compressible, unsteady numerical simulations. (a) Mach contour profiles of the plate shock dynamics. Mach contour range is from Mach 0 to 11. (b) Nondimensional ground pressure profiles as a function of nondimensional distance from the centerline during four stages of the plate shock collapse process: quasi-steady state regime (28 ms); P_C ramp down (54 ms); plate shock collapse (61 ms); and complete P_C ramp down (92 ms). The P_C profile for this case has a pulse width of 45 ms representative of the Phoenix pulse-modulated engines during the terminal descent phase of EDL.

sient ground pressure overshoots were observed with a maximum centerline pressure of 40 kPa ($P_s/P_{C\text{-}max}$ = 0.032) and a duration between 10 and 15 ms. This also developed during P_C ramp up and ramp down phases (M. Mehta and N. O. Renno, manuscript in preparation, 2008).

[42] Figure 6b shows the spatial ground pressure profiles at varying stages of the thruster impingement process. It indicates that the small ground pressure peak of 21 kPa ($P_s/P_{C\text{-}max}$ = 0.017) at r/D_e = 0.9 is observed during the quasi-steady state regime. Minor pressure perturbations of approximately 2.1–3.8 kHz were also observed during this regime (M. Mehta and N. O. Renno, manuscript in preparation, 2008). During the ground pressure overshoot regime when P_C ramp down first occurs, a monotonic spatial decrease in centerline pressure is observed with a maximum of 35 kPa ($P_s/P_{C\text{-}max}$ = 0.028) at t = 61 ms (Figure 6b). As qualitatively observed in our experimental results, the spatial ground pressure is relatively constant in the quasi-steady state regime at approximately 16 kPa ($P_s/P_{C\text{-}max}$ = 0.013) up to a nondimensional radial distance of approximately r/D_e = 0.9 at t = 28 ms. During P_C ramp down, the centerline pressure decreases to approximately 12.4 kPa ($P_s/P_{C\text{-}max}$ = 0.01) and is relatively constant up to approximately r/D_e = 0.9 at t = 54 ms. During complete P_C ramp down, where the thruster inlet stagnation pressure is below 25% of it's maximum value, there is a small monotonic pressure profile with a maximum nondimensional ground pressure of 0.002 (Figure 6b) at the centerline.

5.4. Interpretation of Experimental and Numerical Results

[43] Results of the cold flow test bed and CFD simulations are consistent with each other [*Mehta et al.*, 2007]. These results also agree well to numerical analyses conducted for the actual Phoenix pulsed rocket motors obtained from hot fire tests [*Gulick et al.*, 2006]. Both laboratory and numerical results suggest that a highly unstable normal plate (bow) shock and stagnation bubble form and collapse at the ground during the engine startup and shutdown portions of each power cycle, respectively (Figure 6a). A stagnation

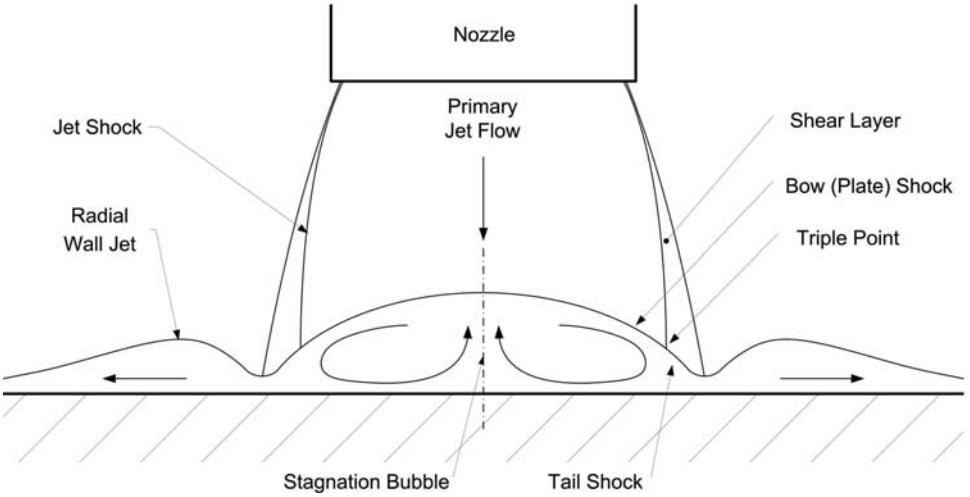

Figure 7. Schematic of supersonic underexpanded jet impingement flow structures [*Pattison et al.*, 2007].

bubble is a subsonic recirculation region below the plate shock (Figure 7) [*Krothapalli et al.*, 1999]. The large pressure overshoots at the ground (Figure 4) are probably associated with the formation and collapse of this plate shock. The amplitude of the largest pressure overshoots depend on the stagnation pressure rise and fall rates, atmospheric density, and the strength of the plate shock. The ground pressure fluctuations during the quasi-steady phase increase as we increase the thruster to ground height due to a weaker and more unstable developed plate shock (not shown) (M. Mehta and N. O. Renno, manuscript in preparation, 2008). From Figures 5 and 6b, it can also be seen for a 1/2 scale thruster, the fully developed plate shock diameter is approximately 5 cm.

[44] From Figure 6a and 7, the other flow features directly related to this interaction during the quasi-steady state regime are symmetric tail shocks that emanate from the triple point and impinge on the surface [*Krothapalli et al.*, 1999]. The triple point region is where the reflected incident (jetshock), plate and tail shocks converge (Figure 7). The small ground pressure peak of 21 kPa ($P_s/P_{C\text{-}max}$ = 0.017) observed at r/D_e = 0.9 in Figure 6b probably resulting from tail shock impingement [*Krothapalli et al.*, 1999] and the relatively constant spatial ground pressure profile along the span of the plate shock diameter (Figures 5 and 6b) are indicative that a fully developed plate shock has formed near the surface.

[45] Although the ground pressure values are different due to different h/D_e cases, an important finding is that the general temporal and spatial ground pressure profile trends are the same for two different altitudes. From the Mach contours, the plume impingement at the surface creates a supersonic wall jet that propagates along the ground at Mach 2 (Figures 6a and 7). This is explained in more detail below. The supersonic wall jet can cause considerable soil erosion and dust lifting.

5.4.1. Plate Shock Dynamics

[46] The dynamics of the impingement of a pulsed rocket plume with the surface at low ambient pressure is illustrated in Figure 6a. From our numerical and experimental results, we deduced the following mechanism in this complex interaction (M. Mehta and N. O. Renno, manuscript in preparation, 2008). At the start of the engine duty cycle, P_C ramp up, isentropic expansion waves coalesce into accelerating shock waves, which propagate downward from the converging-diverging nozzle and impinge on the ground [*Courant and Friedrichs*, 1999]. This compression causes an increase in the flow momentum and ground pressure, which is defined as the preplate shock formation stage. An irreversible normal shock forms when the compression waves are reflected by the ground and coalesce at a particular stand-off distance (shock height above the ground) [*Lamont and Hunt*, 1980]. The nonisentropic behavior and viscous dissipation across the shock boundary causes the ground total pressure to decrease, attributed to a decrease in plume velocity across the shock boundary [*Anderson*, 2004]. The decrease in the total pressure across the plate shock is directly a function of the shock strength (Mach number) [*Lamont and Hunt*, 1980]. Additional ground pressure perturbations are caused by instabilities at the boundaries of a stagnation bubble and plate shock that forms during the quasi-steady portion of the duty cycle (20 to 60 ms during the first cycle and 115 to 150 ms during the second cycle all illustrated in Figure 4). Plate shock fluctuations normal to the surface also contribute to the ground pressure perturbations [*Henderson et al.*, 2005]. These fluctuations are not readily observed in the experimental data because of the limited sampling rate (Figure 4) but are observable to a limited degree in our numerical simulations. Theoretically, as the stand-off distance of the plate shock decreases, the ground pressure increases due to smaller gas expansion over a smaller plume volume below the plate shock. When, on the other hand, the stand-off distance increases, the ground pressure decreases because of an increase in the plume volume below the plate shock which facilitates momentum dissipation. Once the thruster inlet stagnation pressure to ambient pressure ratio is not large enough to support a normal shock at the surface during P_C ramp down phase, the plate shock and/or stagnation bubble collapses, leading to the propagation and impingement of weak shock waves. Through gas compression, this considerably increases the ground pressure similar to the mecha-

nisms described above (M. Mehta and N. O. Renno, manuscript in preparation, 2008). From our results, this mechanism causes large pressure spikes observed at the beginning and end of each engine power cycle (Figure 4). Once the plate shock is absent during complete P_C ramp down, the ground pressure monotonically decreases with decreasing thruster inlet stagnation pressure as would be seen for subsonic jet impingement (Figure 6b) [*Donaldson et al.*, 1971]. The plate shock acts to decelerate the jet flow impingement and leads to a decrease in the ground pressure.

[47] The plate shock dynamics can also be seen by spatial ground pressure profiles (Figures 5 and 6b). As described above, once a plate shock is fully developed, the ground pressure at the centerline drops and remains relatively constant along the plate shock diameter. Once preplate shock formation (Figure 5) and postcollapse (Figure 6b) occur, a monotonic increase in spatial ground pressure is observed due to direct shock wave impingement. This further validates the dynamic process of the normal standoff shock due to pulsed underexpanded jet impingement at low ambient pressure.

5.4.2. Site Alteration and Dust Lifting

[48] Various mechanisms due to the pulsed rocket plume scheme can lead to significant soil erosion and dust lifting. The pressure overshoots described above and the high surface shear stress associated with the supersonic wall jets can lead to soil erosion and dust lifting. Wall jet propagation is caused by the expansion of the jet, developing mainly from tail shock impingement along the surface (Figure 6a) [*Carling and Hunt*, 1974]. Large and rapid pressure fluctuations might cause soil liquefaction [*Youd and Idriss*, 2001]. Ground shock vibrations caused by these large transient pressure overshoots superimposed by the pulsing quasi-steady state overpressure regions may disrupt the soil and break the particle-to-particle cohesive forces. This decreases the bearing capacity and increases the fluidization of the soil and eventually leads to lateral ground failure and crater formation [*Hryciw et al.*, 1990]. This similar mechanism provides a hydraulic mining pulsed water jet to excavate heavy granular and rock material [*Kolle*, 1994]. The extent of ground failure depends on the soil properties, ground impingement pressure, ground shear stress [*Romine et al.*, 1973] and the dynamic interactions between the thruster plume and the ground [*Youd and Idriss*, 2001]. The Martian soil ground pressure threshold before erosion takes place is approximately 3 kPa [*Romine et al.*, 1973]. Also, depending on the plume compression and expansion regions near the surface which behaves nonlinearly with altitude, the overshoot and quasi-steady state ground pressure can significantly change in magnitude as can be seen for the two nondimensional altitude cases presented here: $h/D_e = 8.4$ and 25.

[49] There are three main mechanisms that lead to extensive site alteration and dust lifting [*Romine et al.*, 1973]: (1) bearing capacity failure, (2) viscous erosion, and (3) diffused gas erosion. Through extensively developed scaling laws which address these three mechanisms, we can properly scale Earth gravity based tests for Mars conditions (M. Mehta and N. O. Renno, manuscript in preparation, 2008). All three mechanisms will play a significant role in the site alteration and dust lifting due to Phoenix's pulsed thrust impact on the surface. Also, the recent discovery that Mars northern polar region surface has extensive soil depth variability ranging from 5 cm to greater than 20 cm [*Bandfield*, 2007] has made understanding site alteration and dust lifting important for Phoenix science operations.

6. Planned Future Work

[50] We are planning to use the data presented here to test the effects of NH_3 adsorption on a cross section of Mars stimulant soils. The test are designed to provide information as to what effects such adsorption may have on the chemical analyses that will be performed by the Wet Chemistry Laboratory (WCL) on Phoenix.

[51] We are planning to conduct experiments with our CFTB at the NASA Ames Planetary Aeolian Laboratory (PAL) Mars chamber (Aeolian wind facility) to quantify soil erosion and uplifting during spacecraft landing on Mars (M. Mehta and N. O. Renno, manuscript in preparation, 2008). Our main goal is to understand the flow physics and the effects of the pulsed underexpanded rocket exhaust impinging on the Martian soil. We will use scaling laws (see section 5.1.2) to relate experimental results to the potential site alteration of Phoenix's pulsed rocket plumes at the landing site.

[52] These experimental results will provide the Phoenix Science Team with a first-order approximation to the crater contour as well as the crater depth and dust deposition at the landing site. Results from the tests will be primarily used for scientific interest, providing information about possible dust contamination in the sampling areas for MECA and TEGA, on calibration targets, and general albedo-induced changes to the thermal properties of the science deck [*Marshall et al.*, 2007]. Subsequently, these tests can also be valuable for determining if significant erosion or deposition occurs at the digging location. Since MECA only has four sample analysis opportunities for the wet chemistry cells, it seems important that we understand soil disturbance in the digging area, both its lateral and vertical extent. These top few centimeters are also the zone of chemical contamination from the plumes that could potentially influence TEGA results. Results from these tests can therefore lead to mitigation strategies still within the flexibility of our operational (digging) schemes [*Marshall et al.*, 2007].

7. Conclusion

[53] The FTIR and GC-MS analysis of the thruster plume gases show no detectable hydrazine. This is the primary result of the FTIR and GC/MS analysis, since the presence of hydrazine has the potential to significantly complicate the interpretation of the in situ analysis of the Martian soil. The analysis however did show significant amounts of NH_3 and N_2. The N_2 posses no problem for the Phoenix wet chemistry, but the presence of NH_3 in the plume must be further investigated and a good understanding of the possible reactions obtained.

[54] Our experiments and numerical simulations suggest that the ground impingement pressure of the Phoenix thruster plumes at the surface of Mars generates large transient pressure overshoots which correlates to a ground shock frequency of approximately 20 Hz and a 10 Hz quasi-steady state ground pressure perturbation. These large

ground pressure overshoots potentially occur due to the formation and collapse of the plate shock and stagnation bubble near the surface due to high instability in the plate shock dynamics during P_C start up and shutdown cycles. This has the potential to significantly increase soil erosion and uplifting. The amount of cratering and soil uplifting depends on the soil properties, ambient pressure and engine thrust. Experiments with University of Michigan's cold flow thruster at the NASA Ames Aeolian wind facility will be used to quantify soil erosion and uplifting before Phoenix lands on Mars. The results of this experiment will be used to refine the landing and digging strategy so that contamination processes can be properly understood and mitigated if necessary. This will also describe the jet-induced soil dynamic processes taking place at the landing site during the landing phase of the spacecraft.

[55] **Acknowledgments.** This work was supported by NASA Jet Propulsion Laboratory and the Phoenix Mars Mission. In particular, we would like to thank Peter Smith (Phoenix Mission PI) of University of Arizona; Robert Shotwell (Project Systems Engineer), Rob Grover (EDL Systems Lead) and Mike Hecht (MECA Lead) of NASA JPL; Bill Boynton (TEGA Lead) of University of Arizona; Greg McAllister, Tim Fisher, Pete Huseman, Doug Gulick, and Tim Priser of Lockheed Martin Space Systems; Matt Dawson of Aerojet, Inc.; Chuck Davis of KSC; John Marshall of SETI; Ron Greeley of Arizona State University; Ray Arvidson of Washington University; and Jasper Kok and Robb Gillespie of the University of Michigan for all their support and guidance.

References

Albee, A., S. Battell, R. Brace, G. Burdick, P. Burr, and J. Casani (2000), Report on the loss of the Mars Polar Lander and Deep Space 2 missions, *Rep. JPL D-18709*, Jet Propul. Lab. MPL Invest. Board, Pasadena, Calif.

Anderson, J. D. (2004), *Modern Compressible Flow*, McGraw-Hill, New York.

Bandfield, J. L. (2007), High-resolution subsurface water-ice distributions on Mars, *Nature*, *447*, 64–65, doi:10.1038/nature05781.

Carling, J. C., and B. L. Hunt (1974), The near wall jet of a normally impinging, uniform axisymmetric, supersonic jet, *J. Fluid Mech.*, *66*, 159–176, doi:10.1017/S0022112074000127.

Clark, L., and W. Conner (1969), Exploratory study of scaled experiments to investigate site alteration problems for Martian soft-lander spacecraft, *NASA LWP-765*, NASA Langley Res. Cent., Hampton, Va.

Courant, R., and K. O. Friedrichs (1999), *Supersonic Flow and Shock Waves*, *Appl. Math. Sci. Ser.*, vol. 21, Springer, New York.

Donaldson, C. D., R. S. Snedecker, and D. P. Margolis (1971), A study of free jet impingement. part 2: Free jet turbulent structure and impingement heat transfer, *J. Fluid Mech.*, *45*, 477–512, doi:10.1017/S0022112071000156.

Grover, M. R., T. A. Priser, T. D. Gasparinni, and D. Sabahi (2005), Phoenix EDL critical design review report, paper presented at NASA Phoenix CDR Meeting, NASA Jet Propul. Lab., Pasadena, Calif.

Gulick, D. S., M. Mehta, J. V. Bomba, D. P. Mayfield, P. G. Huseman, and N. O. Renno (2006), Plume/soil interaction data and analysis, paper presented at Phoenix EDL Terminal Descent Sub-Phase Technical Interchange Meeting (TIM), Lockheed Martin Space Syst. Co., Denver, Colo.

Henderson, B., J. Bridges, and M. Wernet (2005), An experimental study of the oscillatory flow structure of tone-producing supersonic impinging jets, *J. Fluid Mech.*, *542*, 115–137, doi:10.1017/S0022112005006385.

Hryciw, R. D., S. Vitton, and T. G. Thomann (1990), Liquefaction and flow failure during seismic exploration, *J. Geotech. Eng.*, *116*, 1881–1899, doi:10.1061/(ASCE)0733-9410(1990)116:12(1881).

Huseman, P. G., and J. Bomba (2000), CFD analysis of terminal descent plume impingement for Mars landers, paper presented at 34th AIAA Thermophysics Conference, Am. Inst. of Aeron. and Astron., Denver, Colo.

Janos, J. J., and S. Hoffman (1968), Forces and moments produced by air and helium jets exhausting parallel to a flat plate in a near vacuum, *NASA Tech. Note*, *TN D-4408*.

Kolle, J. J. (1994), Developing a hydraulic pulse generator, *Mech. Eng. CIME*, [online] 1–7.

Kounaves, S. P., et al. (2008), The 2007 Phoenix Mars Scout Lander MECA Wet Chemistry Laboratory, *J. Geophys. Res.*, doi:10.1029/2007JE003012, in press.

Krothapalli, A., E. Rajkuperan, R. Alvi, and L. Lourenco (1999), Flow field and noise characteristics of a supersonic impinging jet, *J. Fluid Mech.*, *392*, 174–188.

Lamont, P. J., and B. L. Hunt (1980), The impingement of underexpanded axisymetrical jets on perpendicular and inclined flat plates, *J. Fluid Mech.*, *100*, 471–475, doi:10.1017/S0022112080001255.

Land, N., and H. Scholl (1966), Scaled LEM jet erosion tests, *NASA Langley Working Papers*, *LWP-252*, NASA Langley Res. Cent., Hampton, Va.

Lyon, W. C. (1971), Monopropellant thruster exhaust effects on spacecraft, *J. Spacecr. Rockets*, *8*, 689–701.

Markham, J. R., P. M. Bush, P. J. Bonzani, J. J. Scire, V. A. Zaccardi, P. A. Jalbert, M. D. Bryant, and D. G. Gardner (2004), Integrated gas analyzer for complete monitoring of turbine engine test cells, *Appl. Spectrosc.*, *58*, 130–136, doi:10.1366/000370204322729568.

Marshall, J., M. Mehta, and N. O. Renno (2007), Phoenix touchdown tests, NASA Phoenix Project Internal Report, NASA Jet Propul. Lab., Pasadena, Calif.

McBride, B. S., and S. Gordon (1996), Computer program for calculation of complex chemical equilibrium compositions and applications II, Users manual and program description, *NASA Ref. Publ.*, *1311*.

Mehta, M., N. O. Renno, A. J. Cotel, and M. R. Grover (2007), Characteristics of the impingement dynamics of pulsed rocket plumes with the ground at low ambient pressure, paper presented at 43rd AIAA/ASME/SAE/ASEE Joint Propulsion Conference and Exhibit, Am. Inst. of Aeron. and Astron., Cincinnati, Ohio.

Pattison, C. S., S. Cellota, R. Morgan, M. Bray, and W. O'Neill (2007), Cold gas dynamic manufacturing: A non-thermal approach to freeform fabrication, *Int. J. Mach. Tools Manuf.*, *47*, 627–634, doi:10.1016/j.ijmachtools.2006.05.001.

Plemmons, D., K. Wilcher, L. Tamppari, P. Smith, and L. Peach (2007), Spectroscopic plume analysis of the Phoenix Mars Lander hydrazine monopropellant thrusters, paper presented at 43rd AIAA/ASME/SAE/ASEE Joint Propulsion Conference and Exhibit, Am. Inst. of Aeron. and Astron., Cincinnati, Ohio.

Roberts, B., R. O. Wallace, and J. L. Sims (1982), Plume base flow simulation technology, *NASA Tech. Rep.*, *TR-19820023542*.

Romine, G. L., T. D. Reisert, and J. Gliozzi (1973), Site alteration effects from thruster exhaust impingement during a simulated Viking Mars landing: Nozzle development and physical site alteration, NASA Contractor Report, *NASA CR-2252*, Martin Marietta Corp., Denver, Colo.

Sayer, C. F. (1970), The decomposition of hydrazine on the Shell 405 catalyst, paper presented at AIAA 6th Propulsion Joint Specialist Conference, Am. Inst. of Aeron. and Astron., San Diego, Calif.

Wong, E., and J. P. Masciarelli (2002), Autonomous guidance and control design for hazard avoidance and safe landing on Mars, paper presented at AIAA Atmospheric Flight Mechanics Conference, Am. Inst. of Aeron. and Astron., Monterrey, Calif.

Youd, T. L., and I. M. Idriss (2001), Liquefaction resistance of soils: Summary report from the 1996 NCEER and 1998 NCEER/NSF workshops on evaluation of liquefaction resistance of soils, *J. Geotech. Geoenviron. Eng.*, *127*, 297–313, doi:10.1061/(ASCE)10900241(2001)127:4(297).

B. C. Clark, Lockheed Martin Corporation, 10890 Park Range Road, Littleton, CO 80127, USA.

S. P. Kounaves and S. M. M. Young, Department of Chemistry, Tufts University, Medford, MA 02155, USA.

M. Mehta, Department of Atmospheric, Oceanic and Space Sciences, 2215 Space Research Building, University of Michigan, 2455 Hayward Street, Ann Arbor, MI 48109, USA.

L. L. Peach Jr., Universities Space Research Association, 660 Breton Place, Arnold, MD 21012, USA.

D. H. Plemmons, Aerospace Testing Alliance, 1099 Schriever Ave., Arnold AFB, TN 37389-9013, USA. (david.plemmons@arnold.af.mil)

N. O. Renno, Department of Atmospheric, Oceanic and Space Sciences, 1531C Space Research Building, University of Michigan, 2455 Hayward Street, Ann Arbor, MI 48109, USA.

L. Tamppari, Jet Propulsion Laboratory, California Institute of Technology, 480 Oak Grove Drive, Mail Stop 264-623, Pasadena, CA 91109, USA.